ULB

von Karman Institute

Home Page

Title Page

Contents

Page 1 of 41

Go Back

Full Screen

Close

Quit

Successful integration of CFD and experiments in fluid dynamics: the computational investigator point of view

G. Degrez[⋆,†], W. Dieudonné[⋆], T. Magin[⋆,†]

gdegrez@ulb.ac.be

[⋆]von Karman Institute for Fluid Dynamics

[†]Service de Mécanique des fluides, Université Libre de Bruxelles

"Integrating CFD and Experiments in Aerodynamics" Symposium

University of Glasgow, Sep. 8th–9th, 2003

Contents

ULB

von Karman Institute

Home Page

Title Page

Contents

Page 2 of 41

Go Back

Full Screen

Close

Quit

4 Conclusions

1 Introduction

Over the past 30 to 40 years, revolution in scientific and engineering practise brought by the tremendous development of numerical simulation.

In aerodynamics, CFD is now ubiquitous in research and design.

But development of CFD so fast that standards of good use have not emerged yet, or at least are not widespread.

A fundamental question: reliability of numerical simulations $\Rightarrow$ important development of verification and validation (V & V) activities, elaboration of V & V standards.

ULB

von Karman Institute

A trend in CFD simulations: increasingly complex physical problems: 2-phase flows, reacting flows, high temperature flows, complex turbulent flows, which require increasingly complex physical models. Integrated computational and experimental studies very useful to calibrate physical models, for parameter identification problems.

Contents of the talk

- Validation study: hypersonic flow over a blunted cone/flare,
- Flows in inductively coupled plasma (ICP) facilities for thermal protection material (TPM) testing:
  - determination of a TPM sample catalytic activity,
  - analysis of pitot pressure measurements with a cooled pitot probe.

ULB

von Karman Institute

2 Hypersonic flow over a blunted cone-flare

Rationale:

- flow problem exhibiting several features of flows over reentry vehicles,
  - bow shock wave & associated entropy layer,
  - shock induced separation.
- axisymmetric flow problem, to allow thorough grid refinement study

ULB

von Karman Institute

2.1 Wind tunnel, model & experimental techniques

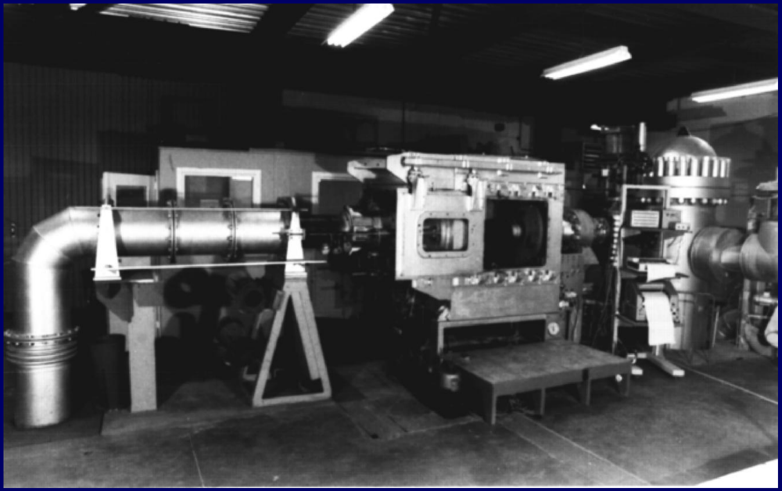

Figure 1: VKI H3 hypersonic wind tunnel

P_0	T_0	M_∞
1.064 MPa	550 K	6

Table 1: Operating conditions

ULB
von Karman Institute

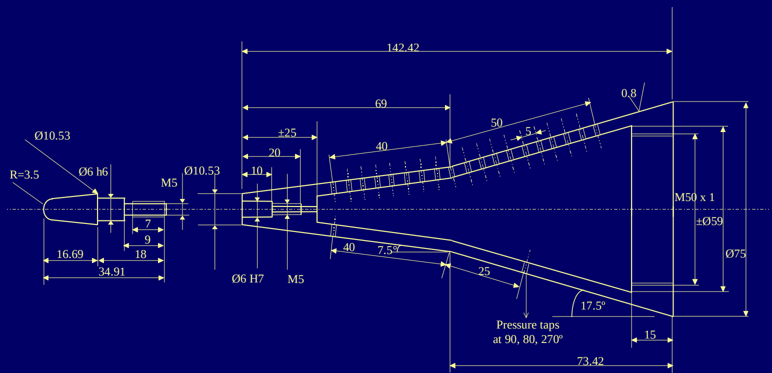

Figure 2: Blunt cone-flare model with pressure taps location

Experimental techniques

Pressure	Electronic pressure scanner	$\delta p = 7.3\%$
Heat fluxes	IR thermography	$\delta St = 11.5\%$

ULB

von Karman Institute

Home Page

Title Page

Contents

Page 8 of 41

Go Back

Full Screen

Close

Quit

2.2 Checking flow axisymmetry & repeatability

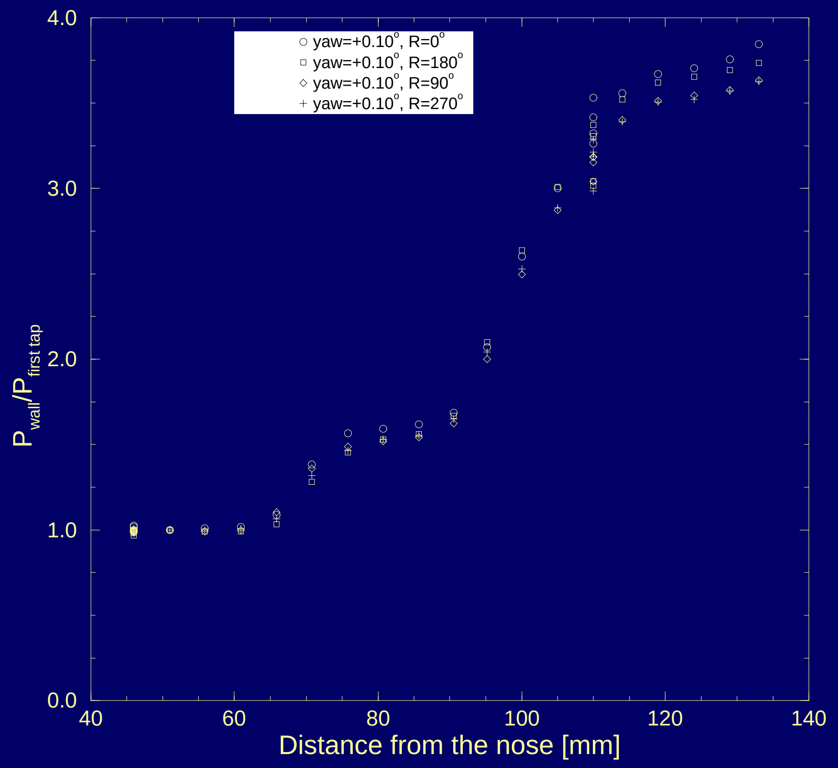

Figure 3: Pressure distributions for 4 azimuthal positions

Sensitivity to pitch/yaw

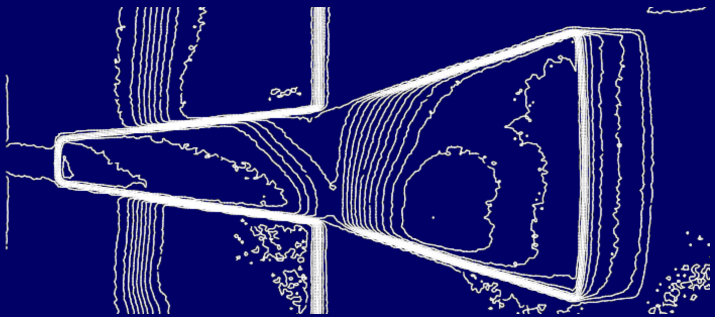

Figure 4: Effect of yaw (0.25°) on IR thermogram

ULB

von Karman Institute

Home Page

Title Page

Contents

Page 10 of 41

Go Back

Full Screen

Close

Quit

Repeatability

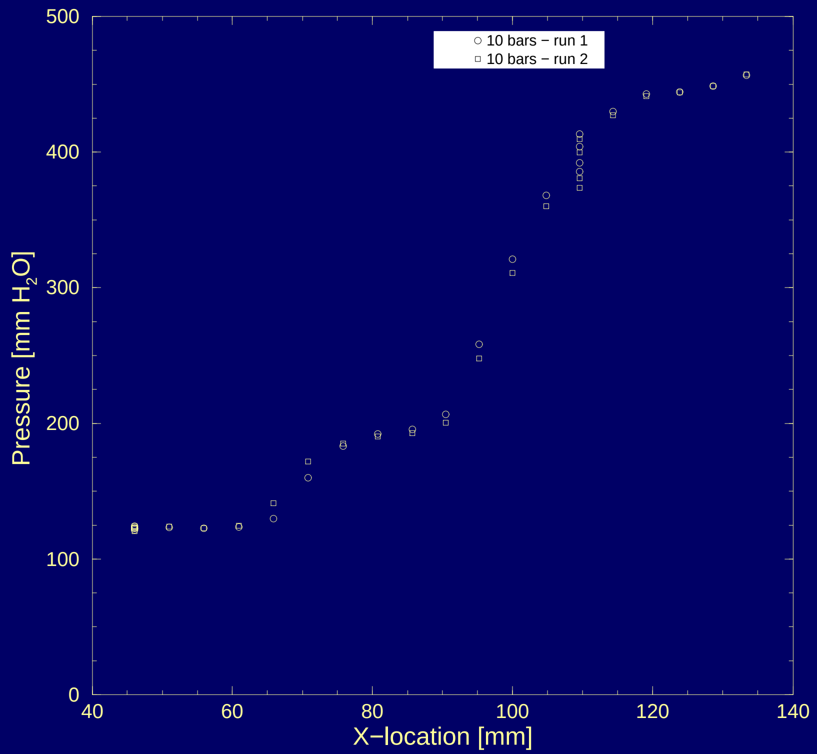

Figure 5: Repeatability of consecutive runs

2.3 Numerical method

- Multiblock structured cell-centered 2D/axisymmetric finite volume solver
- Inviscid fluxes discretized using upwind Riemann solvers. Hybrid upwind splitting scheme used in present study
- algebraic, one-equation and two-equation turbulence models implemented. Spalart-Allmaras turbulence model used for the wind tunnel nozzle flow computations.

Grids

Grid level	coarse	medium	fine
Size	101×21	201×41	401×81

ULB

von Karman Institute

2.4 Computational results

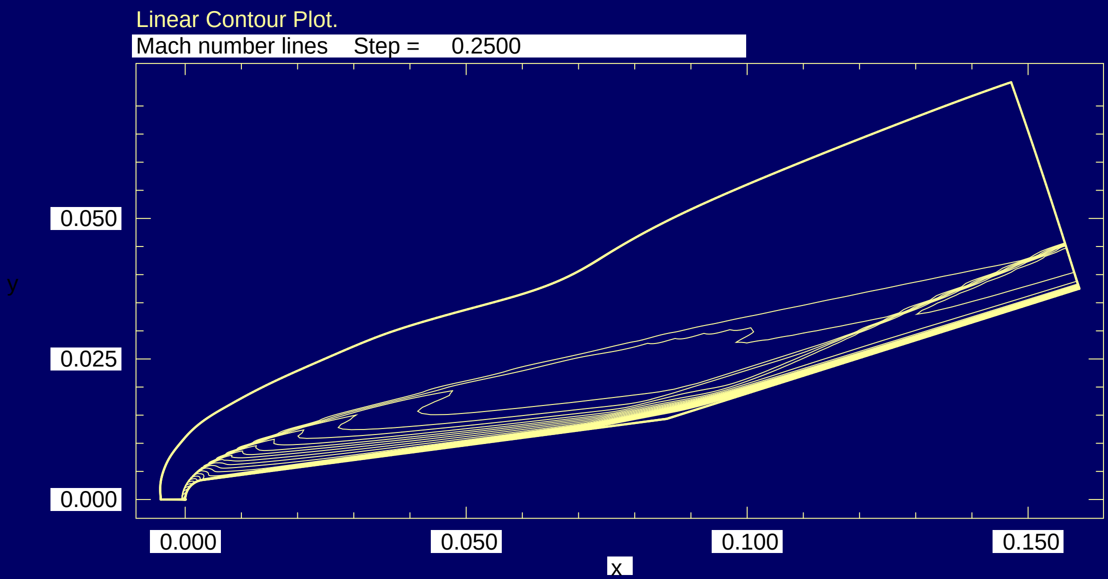

Figure 6: Computed Mach number contours on fine grid

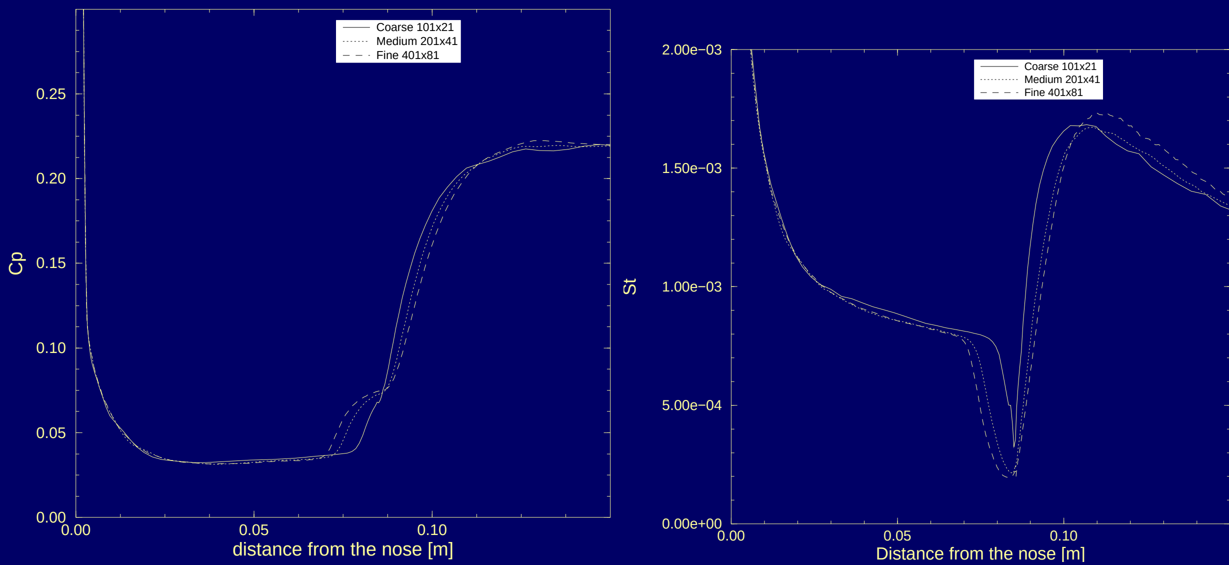

(a) pressure coefficient distribution (b) Stanton number distribution

Figure 7: Computed pressure and heat flux distributions

ULB

von Karman Institute

Home Page

Title Page

Contents

Page 14 of 41

Go Back

Full Screen

Close

Quit

Grid	coarse	medium	fine
x_{sep}/x_{hinge}	0.9496	0.8939	0.8579
x_{reat}/x_{hinge}	1.0491	1.1059	1.1428

Table 2: Separation and reattachment point locations

Conclusion: solution not grid-converged in recirculation bubble/ downstream of reattachment.

ULB

von Karman Institute

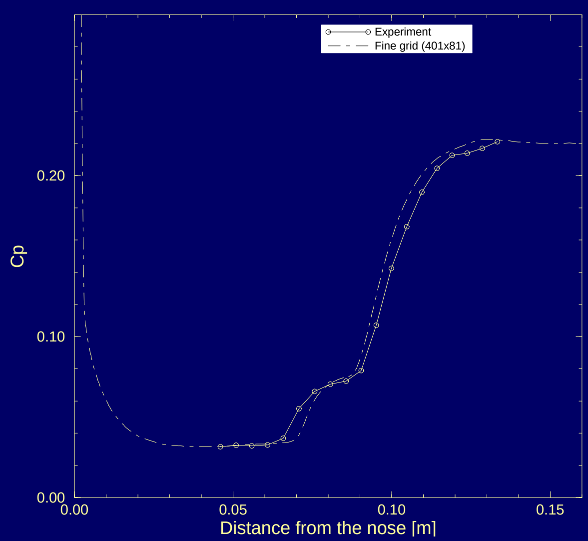

(a) pressure coefficient distribution

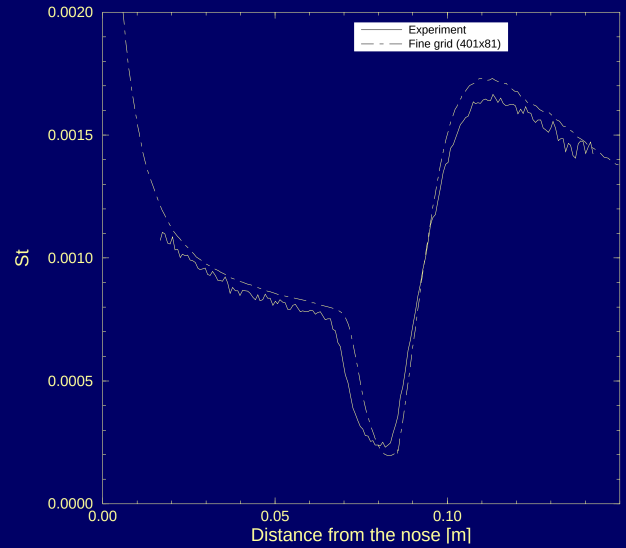

(b) Stanton number distribution

Figure 8: Comparison with experiments

Conclusion: disagreement not only in recirculation region, but also on cone surface (heat flux)

ULB

von Karman Institute

2.5 Effect of freestream non-uniformities

Problem geometry

Figure 9: H3 nozzle geometry

	laminar computations		turbulent computations	
Grid level	Medium	Fine	Medium	Fine
nozzle & test section	415×65	829×129	461×65	921×129
tunnel chamber	45×65	89×129	45×65	89×129

Table 3: Nozzle grids

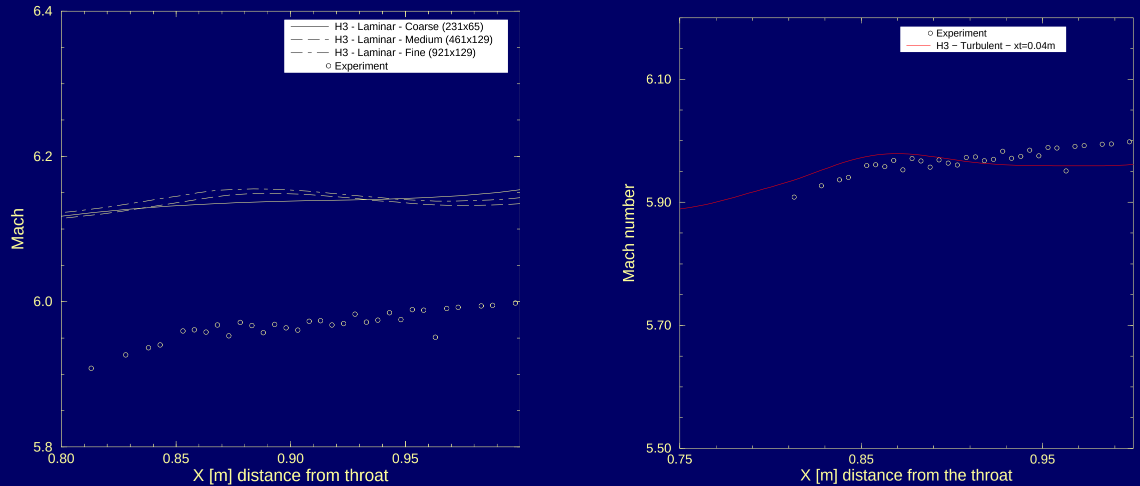

(a) laminar computation (b) turbulent computation

Figure 10: Centerline Mach number distributions

Conclusion: turbulent computation with $x_t = 0.04$ m in agreement with experiments

Confirmation

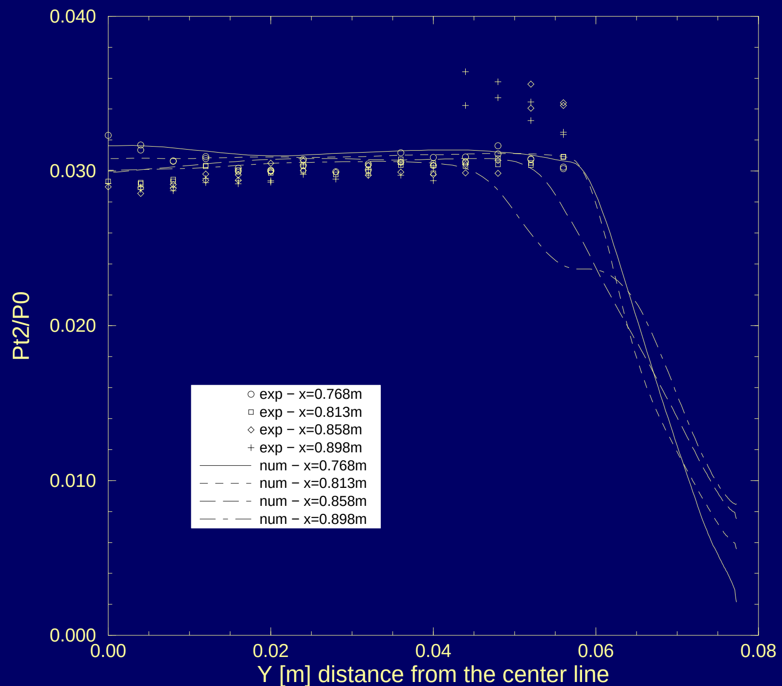

Figure 11: Pitot pressure profiles across jet ($x_t = 0.04$m)

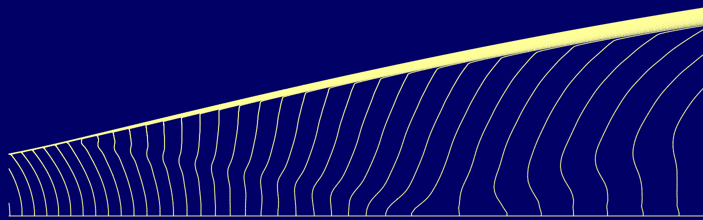

Figure 12: Mach number contours near nozzle throat

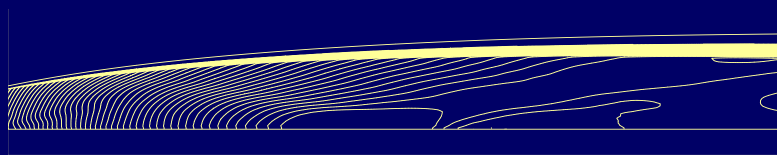

Figure 13: Mach number contours in nozzle

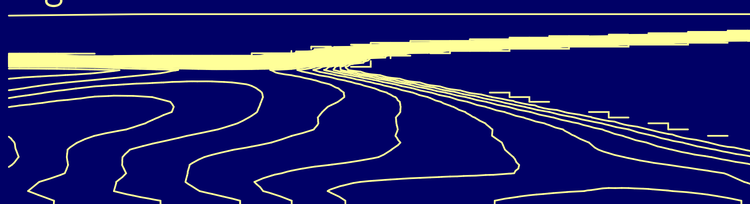

Figure 14: Mach number contours in jet flow

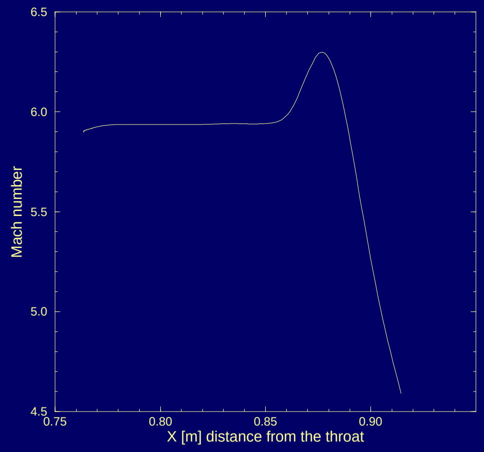

Figure 15: Mach number distribution on cone-flare inflow boundary

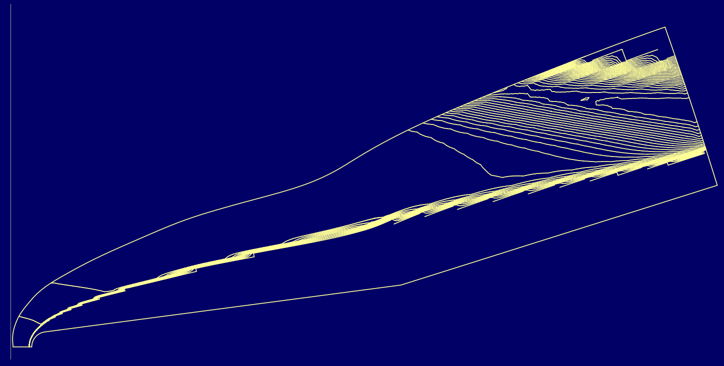

Figure 16: Mach number contours for model in wind tunnel

ULB

von Karman Institute

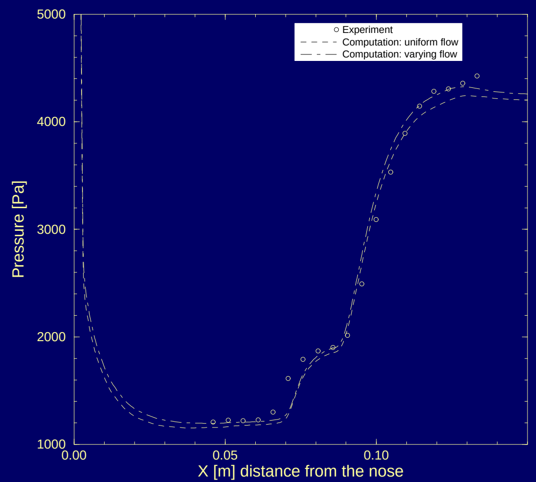

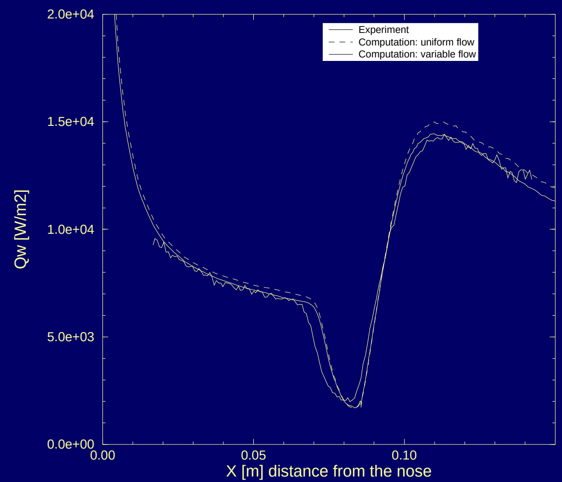

(a) pressure coefficient distribution (b) Stanton number distribution

Figure 17: Comparison with experiments

Observation: computed heat flux on cone in agreement with experiments

Uniform Mach 5.9 inflow conputation

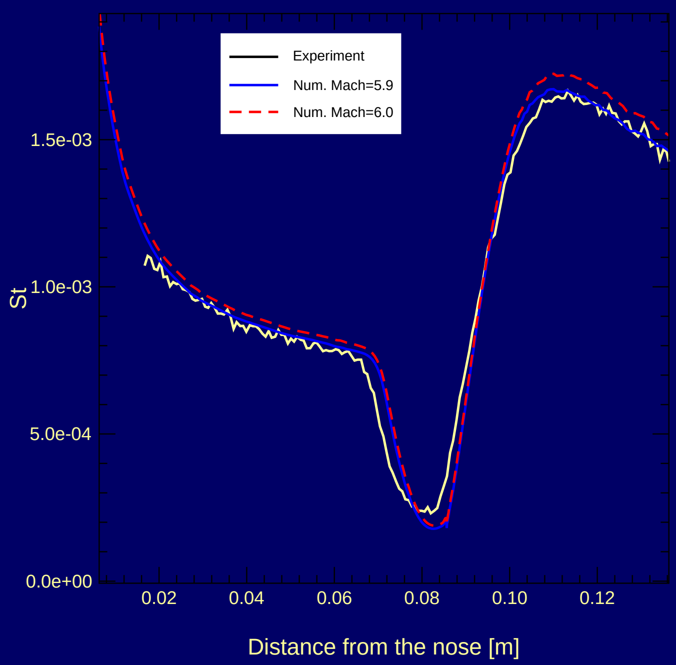

Figure 18: Stanton number distributions, uniform $M_\infty = 5.90$ inflow

3 Flows in ICP facilities

3.1 Determination of wall catalytic efficiency by combined experiments and computations

3.1.1 Motivation

- Re-entry vehicles must be protected by heat shields made of Thermal Protection Materials (TPM);
- Heat shield size controlled by wall heat flux, which strongly depends on the heat shield surface catalytic efficiency.

⇒ Need to know the catalytic efficiency of TPS materials

ULB

von Karman Institute

BUT

- TPS materials catalytic efficiency in flight conditions cannot be reliably calculated a priori using some physico-chemical theory or computational model, or measured directly.

  $\Longrightarrow$ it has to be determined indirectly through its effect on wall heat flux by experimental testing on TPS samples in high enthalpy facilities producing flow conditions close to flight conditions.

- ICP facilities particularly well suited for such testing because of very high chemical purity of the plasmas (absence of metallic impurities due to electrode erosion). $\Longrightarrow$ Motivation for the construction of VKI's large (1.2MW/ 160mm diameter) ICP facility.

ULB

von Karman Institute

3.1.2 The IPM methodology

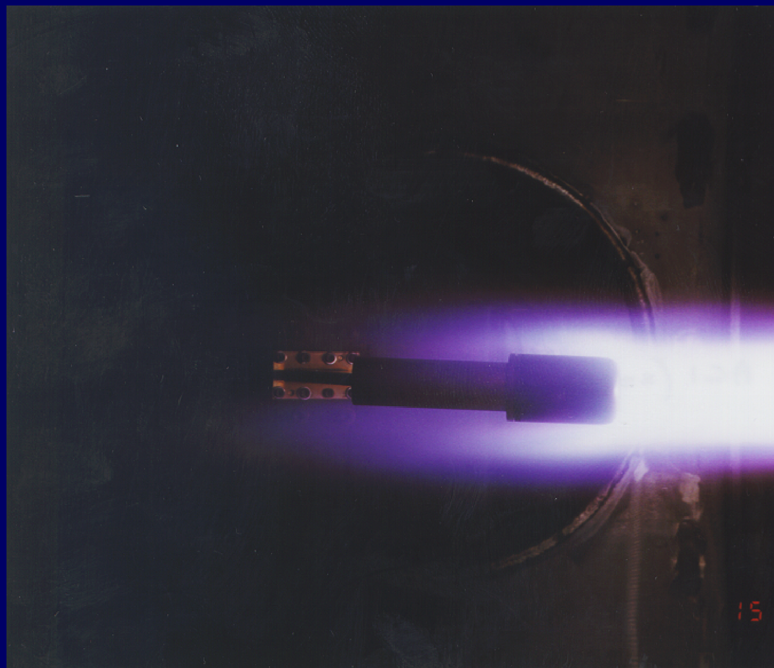

Figure 19: Heat flux probe in VKI Plasmatron (air, $p = 75$ kPa, $P = 250$ kW, $q_m = 8$ gs^{-1}, no swirl)

Assuming the flow to be in LTE outside the thermal/chemical boundary layer around the TPS sample, the stagnation point heat flux can be written as

$$q_w = f(p_e, h_e, (\frac{\partial v}{\partial r})_e, \delta, u_e \frac{\partial}{\partial x}(\frac{\partial v}{\partial r})_e, T_w, \gamma_w) \qquad (1)$$

outer thermodynamic state — radial velocity gradient

boundary layer thickness — axial acceleration

wall properties

$\Rightarrow$ If all other quantities are know, and a model is available to compute the stagnation point heat flux, the catalytic activity γ_w can be determined

- p_e, q_w, T_w measured experimentally,
- other quantities obtained from a LTE flow computation?

ULB

von Karman Institute

ICP facility

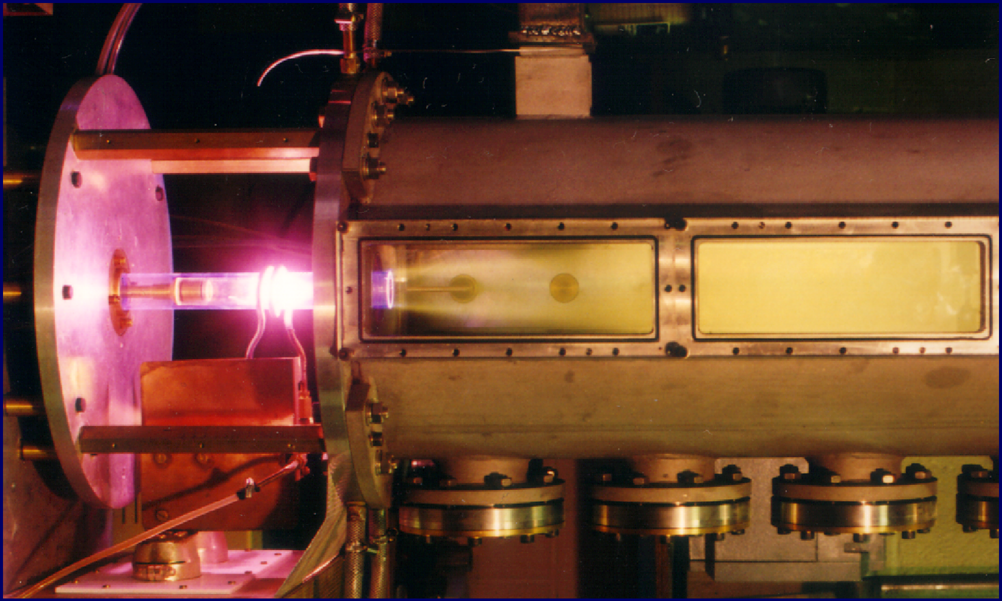

Operational parameters

- mass flow,
- pressure,
- power injected in plasma.

ULB

von Karman Institute

Home Page

Title Page

Contents

Page 28 of 41

Go Back

Full Screen

Close

Quit

LTE flow computational model

- Multiblock coupled hydrodynamic/EM cell-centered finite volume solver,
- 2D (axisymmetric) EM field model (important for low aspect ratio torches)
- 2nd order pressure-stabilized collocated formulation.
- thermodynamic properties computed on-the-fly using statistical thermodynamics; transport properties computed from Chapman-Enskog perturbative theory.

ULB

von Karman Institute

Illustrative result

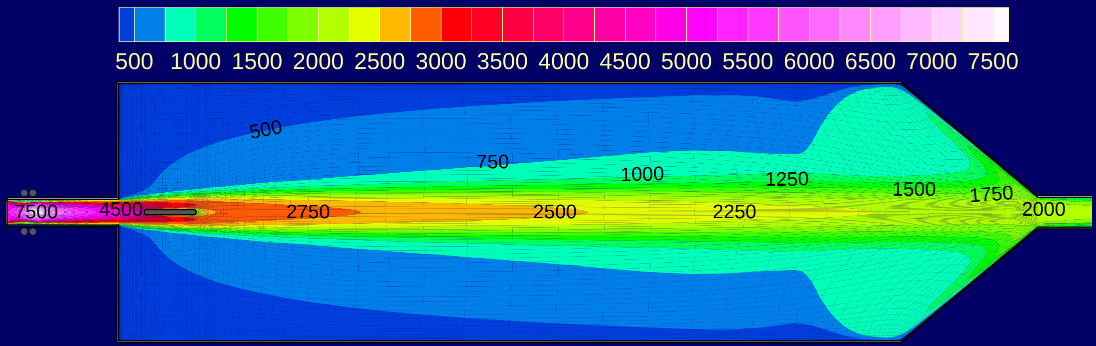

Figure 20: Temperature field in VKI pilot ICP facility (air, $p = 10.13$ kPa, $P = 4$ kW, $q_m = 0.55$ gs^{-1}, no swirl)

Observation: flow pattern depends (almost) exclusively on mass flow

$$\Pi_1 \equiv \frac{\delta}{R}, \qquad \Pi_2 \equiv u_e \frac{\partial}{\partial x}\left(\frac{\partial v}{\partial r}\right)_e / \left(\frac{\partial v}{\partial r}\right)_e^2,$$

independent of pressure/power combinations.

Reconstruction of boundary layer edge properties

Stagnation point heat flux (Eqn 1) can be re-expressed as

$$q_w = f(p_e, h_e, (\frac{\partial v}{\partial r})_e, \Pi_1, \Pi_2, \gamma_w, T_w) \tag{2}$$

Performing an auxiliary heat flux measurement on a on a cold wall ($T_w \sim 300$ to 400 K) reference heat flux probe assumed to be fully catalytic ($\gamma_w = 1$), and the non-dimensional parameters $\Pi_{1,2}$ obtained from an LTE flow simulation, this becomes an equation in 2 unknowns, i.e. h_e and $(\frac{\partial v}{\partial r})_e$.

To close the problem, a second auxiliary measurement is performed, namely a pitot pressure measurement using a cooled pitot probe. In a cold high Reynolds number flow,

$$\Delta p = p_{\text{pitot}} - p = \frac{\rho_e u_e^2}{2}$$

ULB

von Karman Institute

For a cooled pitot probe in a hot low Reynolds number plasma flow

$$\Delta p = K_p \frac{\rho_e u_e^2}{2} \tag{3}$$

where the impact parameter K_p can a priori depend on flow Reynolds number and freestream/wall temperature combination. The relationship between K_p and these parameters was the subject of a specific computational study (section 3.2).

Eqn 3 can be rewritten as

$$\frac{2\Delta p}{\rho_e \left(R(\frac{\partial v}{\partial r})_e\right)^2} = K_p \left(\frac{u_e}{R(\frac{\partial v}{\partial r})_e}\right)^2 \tag{4}$$

where there appears an additional non-dimensional parameter

$$\Pi_4 = \frac{R(\partial v/\partial r)_e}{u_e} \tag{5}$$

which is also obtained from the LTE flow simulation in the ICP facility.

The boundary layer edge enthalpy h_e and velocity gradient $(\frac{\partial v}{\partial r})_e$ can then be reconstructed by solving the system

$$q_{w,\mathrm{aux}} = f((\frac{\partial v}{\partial r})_e, h_e, p_e, \Pi_1, \Pi_2, T_{w,\mathrm{aux}}, \gamma_w = 1) \qquad (6)$$

$$\Delta p = \frac{K_p}{2{\Pi_4}^2}\rho_e(p_e, h_e)\left(R(\frac{\partial v}{\partial r})_e\right)^2 \qquad (7)$$

LTE flow simulation output unknowns
experimental measurements

where the stagnation point heat flux function f is obtained by running a chemical non-equilibrium one-dimensional solver for the self-similar axisymmetric stagnation line flow (4th order compact Hermitian finite difference solver).

ULB

von Karman Institute

Calculation of heat flux abacus (optional)

Run stagnation line flow solver for various T_w, γ_w combinations using the reconstructed boundary layer edge properties

$$q_w = f(p_e, h_e, (\frac{\partial v}{\partial r})_e, \Pi_1, \Pi_2, \gamma_w, T_w)$$

$\longrightarrow$ produce a heat flux abacus.

Determination of TPS material catalytic activity

From experimental measurement of a TPS sample wall temperature and stagnation point heat flux (T_w, q_w)
$\longrightarrow$ deduce γ_w by solving

$$q_w = f((\frac{\partial v}{\partial r})_e, h_e, p_e, \Pi_1, \Pi_2, T_w, \gamma_w) \qquad (8)$$

or graphically from heat flux abacus.

3.1.3 Summary & illustrative application

CATALYTIC ACTIVITY DETERMINATION METHODOLOGY

LTE VISCOUS FLOW SIMULATION

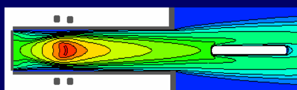

High enthalpy flow simulation around model

3 dimensionless hydrodynamic parameters (Π_i)

EXPERIMENTS

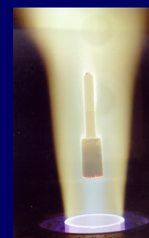

Heat flux (qw) and Pitot presure (ΔP) measurements on a fully catalytic (γw) cold wall model

RECONSTRUCTION OF THE PLASMA JET CHARACTERISTICS (he , dv/dr)

Non−equilibrium BL computation

$$qw_{BL}(he, dv/dr, \Pi_1, \Pi_2, \gamma_w, Tw) = qw)_{exp.}$$

Hydrodynamics

$$\Pi_3 \, \rho_e \, (he, p) \, (R \, dv/dr)^2 = \Delta P_{exp.}$$

Calculation of the wall heat flux for various catalytic efficiency (γw) /wall temperature combinations using non−equilibrium BL solver

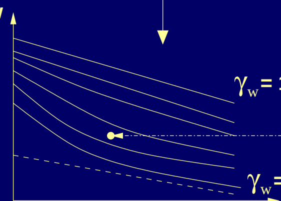

Test measurements on a TPS material sample

catalytic efficiency identification

LTE computation

Input parameters: axial injection, $p = 10$ kPa, $P = 75$ kW, $q_m = 8\ \mathrm{g\,s^{-1}}$.

$$\Pi_1 = 0.372 \qquad \Pi_2 = 2.895 \qquad \Pi_4 = 0.496$$

Heat flux and pitot pressure measurements using a cooled copper probe

Operating conditions: $q_m = 8\ \mathrm{g\,s^{-1}}$, $p = 2.5\ \mathrm{kPa}$, $P_{\mathrm{el}} = 100\ \mathrm{kW}$.

$$p_{\mathrm{pitot}} - p_{\mathrm{ref}} = 25\ \text{Pa},\ q_w = 547.5\ \mathrm{kW\,m^{-2}}$$

Reconstruction of boundary layer edge properties

Using $K_p = 1.1$ and Gupta's chemical reaction model, we find

$$h_e = 13.85\mathrm{MJ\,kg^{-1}}\ \text{and}\ (\partial v/\partial r)_e = 3710\ \mathrm{s^{-1}}$$

ULB

von Karman Institute

Construction of heat flux abacus

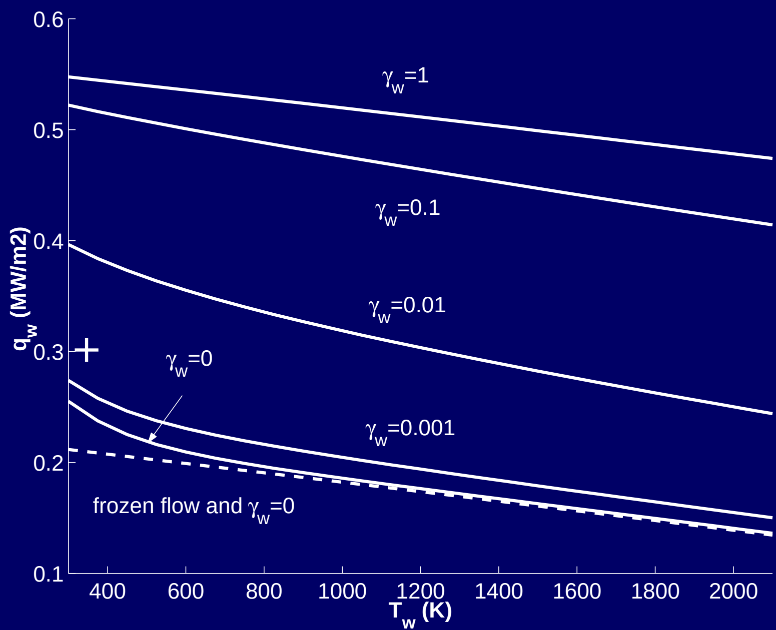

Heat flux abacus for VKI Plasmatron with air, $q_m = 8\ \mathrm{gs}^{-1}$, $p = 2.5\ \mathrm{kPa}$, $P_{\mathrm{el}} = 100\ \mathrm{kW}$

ULB

von Karman Institute

Home Page

Title Page

Contents

◀◀ ▶▶

◀ ▶

Page 37 of 41

Go Back

Full Screen

Close

Quit

TPS testing and determination of catalytic activity

Measurement of heat flux and wall temperature of a quartz sample: $q_w = 301.4\ \mathrm{kW\,m^{-2}}$, $T_w = 346.4\ \mathrm{K}$ (see heat flux abacus).

Iterating with boundary layer solver, we get $\gamma_w = 3\,10^{-3}$

3.2 Numerical study of the flow around a cooled pitot probe

The value of the impact parameter K_p in Eqn. 3 was determined from LTE flow computations. They showed that

- $p_t - p \approx \rho u^2/2 \rightarrow$

$$\frac{p_{\mathrm{pitot}} - p}{p_t - p} \approx \frac{2\Delta p}{\rho_e u_s^2} = K_p$$

ULB

von Karman Institute

Home Page
Title Page
Contents
Page 38 of 41
Go Back
Full Screen
Close
Quit

- K_p increases very slightly with decreasing wall temperature,
- K_p increases with decreasing probe dimensions (low-Reynolds number effect),
- K_p in good agreement with cold flow correlation by Homann.

CAVEAT

In practise, one doesn't measure $\Delta p = p_{\text{pitot}} - p$ but rather the difference between p_{pitot} and some reference pressure (e.g. test chamber pressure). Computational results show that

- for axial injection, $p_{\text{ref}} \approx p$,
- for swirling injection, there can be differences up to 45% between $p_{\text{pitot}} - p$ and $p_{\text{pitot}} - p_{\text{ref}}$.

Correlations for K_p inapplicable for swirling flows

ULB

von Karman Institute

4 Conclusions

Examples of combined CFD and experimental studies carried out in the Aerospace department at the von Karman Institute over the past few years have been presented. The main lessons learned from these studies are the following.

hypersonic flow over a blunted cone/flare validation study

- careful model alignment to ensure flow axisymmetry extremely important;
- accurate knowledge of boundary conditions needed: discrepancies in computed and measured surface heat fluxes shown to be due to freestream non-uniformities.

ULB

von Karman Institute

Flows in ICP facilities

- synergetic use of two CFD models (LTE coupled hydrodynamic/EM solver and 1D chemical non-equilibrium stagnation line solver) and experiments essential to determine TPMs catalytic activity;
- computational study of flow around a cooled pitot probe very useful for the data reduction of pitot pressure measurements

von Karman Institute
Home Page
Title Page
Contents
Page 41 of 41
Go Back
Full Screen
Close
Quit